

## ANALYSIS OF THE SPATIOTEMPORALLY VARYING EFFECTS OF URBAN SPATIAL PATTERNS ON LAND SURFACE TEMPERATURES

Cheng LI<sup>1\*</sup>, Jie ZHAO<sup>2</sup>, Nguyen Xuan THINH<sup>3</sup>, Wenfu YANG<sup>4</sup>, Zhen LI<sup>4</sup>

<sup>1</sup> Department of Geo-Information Science, School of Resources and Geosciences, China University of Mining and Technology, Daxue Road 1, 221116 Xuzhou, Jiangsu, China

<sup>2</sup> Huaihai Institute of Development, Jiangsu Normal University, Heping road 57, 221009 Xuzhou, Jiangsu, China

<sup>3</sup> Department of Spatial Information Management and Modeling, Spatial Planning Faculty, TU Dortmund University, August-Schmidt-Str 10, 44227, Dortmund, Germany

<sup>4</sup> Shanxi Coal Geology Geophysical Surveying Exploration Institute, Yingbinxijie 380, 030600 Jinzhong, Shanxi, China

Received 03 October 2017; accepted 20 December 2017

**Abstract.** Urban heat islands (UHIs) are a worldwide phenomenon that have many ecological and social consequences. It has become increasingly important to examine the relationships between land surface temperatures (LSTs) and all related factors. This study analyses Landsat data, spatial metrics, and a geographically weighted regression (GWR) model for a case study of Hangzhou, China, to explore the correlation between LST and urban spatial patterns. The LST data were retrieved from Landsat images. Spatial metrics were used to quantify the urban spatial patterns. The effects of the urban spatial patterns on LSTs were further investigated using Pearson correlation analysis and a GWR model, both at three spatial scales. The results show that the LST patterns have changed significantly, which can be explained by the concurrent changes in urban spatial patterns. The correlation coefficients between the spatial metrics and LSTs decrease as the spatial scale increases. The GWR model performs better than an ordinary least squares analysis in exploring the relationship of LSTs and urban spatial patterns, which is indicated by the higher adjusted  $R^2$  values, lower corrected Akaike information criterion and reduced spatial autocorrelations. The GWR model results indicate that the effects of urban spatial patterns on LSTs are spatiotemporally variable. Moreover, their effects vary spatially with the use of different spatial scales. The findings of this study can aid in sustainable urban planning and the mitigation the UHI effect.

**Keywords:** land surface temperature, urban spatial pattern, geographically weighted regression, spatiotemporally heterogeneity, scale effect.

### Introduction

As urbanization has occurred, the natural resource base, such as the lands used for agriculture, forests and wetlands, have been replaced by urban lands (Jantz *et al.* 2004). Although urban land covers a very small percentage of the world's land surface in comparison with other land-cover types, their rapid expansion with continued urbanization has had marked effects on the environment and our socio-economy. One particularly significant consequence of urbanization is the formulation of urban heat islands (UHIs), where the atmospheric and surface temperatures above and around densely built cities are higher than those in nearby rural areas (Voogt, Oke 2003). Increased temperatures in urban areas could contribute to increasing water and energy consumption and could result

in alterations in the biotic communities in urban areas (White *et al.* 2002). Additionally, the UHI effect could lead to the increase in the ground level ozone, which directly threatens human health (Akbari *et al.* 2001). In considering rapid urbanization and the importance of UHI effects, monitoring the UHI effects and exploring their characteristics are increasingly important, as is adopting appropriate sustainable land use plans to mitigate UHI effects.

The UHI effect is often captured by land surface temperature (LST) measurements (Kikon *et al.* 2016; Kumar, Shekhar 2015). LST is a key physical indicator of land surfaces directly influenced by urban land-cover changes and has implications for the research of urban climate change (Huang, Cadenasso 2016; Weng 2009). Continual, historical, and precise information about the LST is a prerequisite for further analysis and sustainable development, as

\*Corresponding author. E-mail: [cheng.li@cumt.edu.cn](mailto:cheng.li@cumt.edu.cn)

has been stated previously. Satellite images have become an effective tool for retrieving the LST of wide spatial and temporal regions. The increasing availability of satellite images with significantly improved spectral and spatial resolutions has played an important role in more detailed LST maps. Numerous studies have validated the use of various satellite thermal infrared (TIR) datasets, including AVHRR (Streutker 2002), MODIS (Buyantuyev, Wu 2010), Landsat TM/ETM+ (Zhang *et al.* 2013), ASTER (Mallick *et al.* 2013), supported by their low cost, large area spatial coverages, and high temporal resolutions.

To mitigate the UHI effect, numerous studies have been conducted to investigate the correlation between LST and various spatial factors in different study areas. The spatial patterns of UHIs are affected by weather conditions, land surface characteristics, and human activities (Li *et al.* 2012; Voogt, Oke 2003; Wu *et al.* 2013). Among these factors, land surface characteristics, represented by land use and land cover (LULC), are identified as the main reasons for the UHI effect. The relationship between LSTs and LULC has been the focus of numerous UHI centered studies (Buyantuyev, Wu 2010; Guo *et al.* 2016; Song *et al.* 2014; Zhou *et al.* 2017). LST data derived from remote sensing images capture the radiative energy emitted from the land surface, including that from buildings, vegetation, bare land, and water (Voogt, Oke 2003). Thus, LST could be affected by the spatial patterns of urban areas (Forman 1995). Two types of indicators have been applied to characterize these spatial pattern: spatial compositions (the variety and abundance of patch types) and spatial configurations (the spatial characteristics and arrangements) (Gustafson 1998). Numerous studies were conducted to investigate the qualitative relationships between LSTs and urban spatial patterns. By adopting a sample set, the spatial metric values of each sample can be plotted against the relevant LST values. Different quantitative methods, including Pearson correlations (Li *et al.* 2013), and global regression models (Connors *et al.* 2013), were adopted to measure the extent of the impact of urban spatial patterns of land-cover types on LSTs. A negative correlation has been observed between vegetation abundance and LSTs in urban areas (Li *et al.* 2011; Liang, Weng 2008). However, LSTs are often found to be positively correlated with the percentage of the built-up land (Li *et al.* 2011; Kikon *et al.* 2016). Landscape configurations can influence the energy exchange and the efficiency of surface energy fluxes (Forman 1995; Song *et al.* 2014). Maimaitiyiming *et al.* (2014) indicated that LST is negatively related with vegetation edge density in Aksu City. The patch density of vegetation had a significant negative relationship with LSTs. Increasing the vegetation patch density could result in significantly higher LSTs (Li *et al.* 2012; Zhou *et al.* 2011). Vegetation and impervious surfaces are two key urban components in UHI dynamics (Ridd 1995). There is growing concern about the effects of urban spatial patterns on LSTs, which can help to provide information for urban planning and sustainable development. Furthermore, recent works have

only focused on describing the characteristics of LST distributions and their relationships with underlying determinants for an entire study area. As such, the studies failed to address the spatial heterogeneities in the effects of urban spatial patterns on LSTs. Spatial and temporal heterogeneities usually exist in the relationships between spatial patterns of land-cover types and the local LSTs (Buyantuyev, Wu 2010; Li *et al.* 2011; Zhou *et al.* 2014). In addition, analyzing the LSTs at a single time point would ignore the fact that the area experiencing the most intense UHI effect is not always located at the center of the city, but can change its location with the progression of urbanization. Therefore, the impacts of urban spatial patterns on LSTs cannot be fully understood. To address these gaps in the existing studies, there is an urgent need to quantify the relationships between LSTs and the spatial patterns of land cover considering the spatiotemporal variations of the effects of the driving factors on LST.

Scale is an important aspect of investigating and analyzing the hierarchical organization of the geographic features (Marceau 1999). It has been widely acknowledged that LST and urban spatial patterns are scale-dependent since they change with the scale of the observation or analysis. Therefore, the impacts of different spatial scales on the correlation between urban spatial patterns and LSTs must be analyzed. However, previous studies have mainly examined these relationships for a single scale, which is often dependent on the spatial resolution of the remote sensing and other data sources (Maimaitiyiming *et al.* 2014; Zhou *et al.* 2011).

Using Hangzhou City, China as a case study, the overall objective of this study is to improve the understanding of the spatiotemporal variations of LSTs and the effects of urban spatial patterns on LSTs, as well as to provide recommendations for urban planning in order to mitigate UHI effects. The specific steps in this study are as follows: (1) to derive the multitemporal LST data from remote sensing images for the study area, (2) to quantify the urban spatial patterns using a set of spatial metrics, and (3) to explore the quantitative relationship between LST and urban spatial patterns with consideration of scaling effects and spatiotemporal heterogeneities.

## 1. Study area and material

### 1.1. Study area

Hangzhou City (located between 29°11' and 30°33' N and 118°21' and 120°30' E) is located in the southern part of the Yangtze River Delta (Figure 1). It has a total administrative area of approximately 16,596 km<sup>2</sup>, with 4,876 km<sup>2</sup> designated as the area of the city proper. The city has a northern-monsoon-influenced humid subtropical climate, with an average annual temperature of 15.7–17.2 °C. The annual precipitation varies from 1352 to 1600 mm. The Qiantang River is the major river in this area. Most of the city area is flat, with elevation value ranging from 2 to 10 m. Hilly and mountainous areas account for 29% of

Hangzhou City. The major land-cover types in Hangzhou City include built-up land, farmland, vegetation, and water bodies.

As the capital of Zhejiang Province, Hangzhou is well known as one of the most developed cities in mainland China. Since the implementation of the Reform and Opening policy, Hangzhou City has experienced a rapid urbanization process. Its gross domestic product (GDP) increased from 178 billion RMB in 2002 to 834 billion RMB in 2013, placing it 10th among all cities in China. The population increased by 27.2% from 6.95 million in 2002 to 8.84 million in 2013. The developmental characteristics and land-cover changes in Hangzhou City provide useful representations of the economically developed cities throughout China.

## 1.2. Data

Although most developed countries have comprehensive land-cover information, a relative lack of geospatial data is a common occurrence in developing countries, particularly in China. In addition to the common advantages of remote sensing images, Landsat images, with their medium spatial resolutions and multiple spectra, provide an appropriate data source for land cover and LST studies because they are free and maximize the possible temporal monitoring period (Patino, Duque 2013).

The Landsat Enhanced Thematic Mapper Plus (ETM+) image from July 13, 2002, and Landsat 8 image from July 19, 2013, were acquired from the U.S. Geological Survey (USGS). The related average daily temperatures are 32 °C and 30 °C, respectively. Landsat data were applied for mapping land cover and retrieving the LSTs of the study area. An improved dark-object subtraction atmospheric correction was carried out to eliminate the impact of atmospheric disturbance on the pixel values (Chavez 1988). The calculation of the at-sensor spectral radiance

is conducted to convert the images acquired from multiple sensors into a common radiometric scale. Using the parameters in the metadata, a radiometric calibration was carried out to transform the digital number value for both the reflective and thermal bands into at-sensor radiance values (Eq. (1)). The image processing was performed using the ENVI 5.1 software.

$$L_{\lambda} = \frac{LMAX_{\lambda} - LMIN_{\lambda}}{Q_{calmax} - Q_{calmin}} \times (Q_{cal} - Q_{calmin}) + LMIN_{\lambda}, \quad (1)$$

where  $L_{\lambda}$  represents the spectral radiance value at the sensor's aperture in  $W/(m^2 \cdot sr \cdot \mu m)$ ,  $LMAX_{\lambda}$  and  $LMIN_{\lambda}$  represent the calibration constants of the sensor, which are equal to the maximum and minimum values of the spectral radiance detectable for each band.  $Q_{calmax}$  and  $Q_{calmin}$  are the maximum and minimum calibrated pixel value, respectively.  $Q_{cal}$  represents the quantized calibrated pixel value.

## 2. Methodology

### 2.1. Land cover classification

Maximum likelihood classification (MLC) was applied to conduct the classification. For each image, 40–60 training samples for each class were adopted to train the image. A total of 200 random points generated by stratified random sampling method were adopted to assess classification accuracy. The classified image extracted by MLC include four classes: built-up land, farmland, forest and water body.

Hierarchical classifications are applied to improve the classification accuracy after MLC. The performance of these methods are dependent on the designs of their decision trees, including the tree structures, the choice of the features at each node, and the decision rules (Setiawan et al. 2006; Lu, Weng 2004). Digital Elevation Model

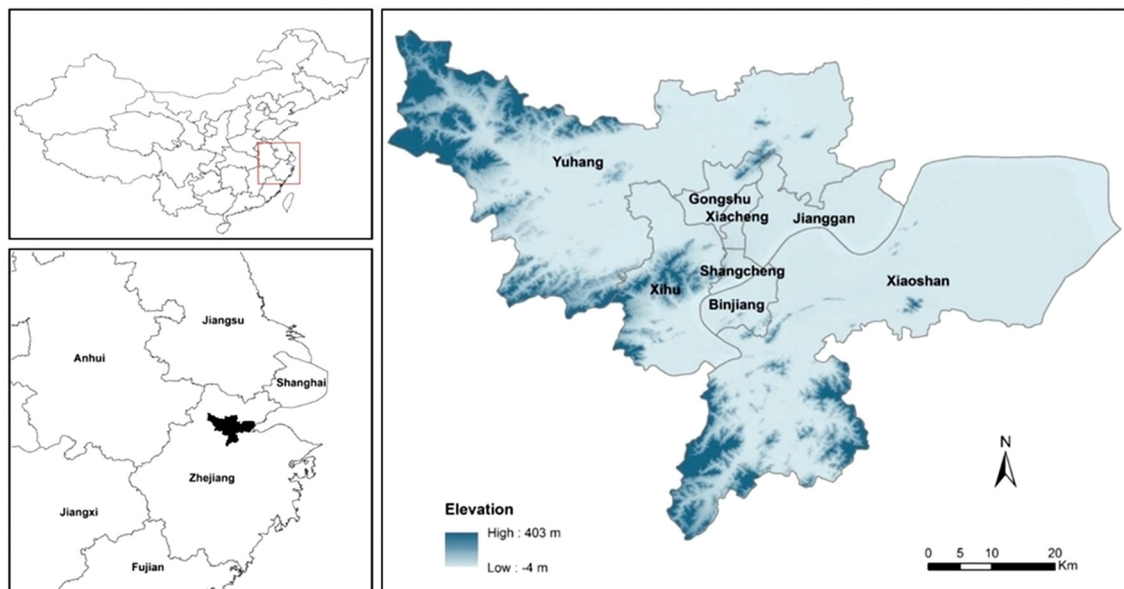


Figure 1. Location of study area (Hangzhou) and its topography

(DEM) as well as the tasseled cap transformation were involved in the decision tree to refine the classification results (Li, Think 2013). The degrees of the slopes were extracted from the DEM data. Farmland and built-up pixels with slopes higher than 10 degrees were reclassified as forest. The brightness band has higher values for surfaces with little or no vegetation; the greenness band is associated with green vegetation; and the wetness band is associated with soil moisture, water, and other moist features. We can refine the classification results through defining the specific rules of the decision tree.

### 2.2. Retrieval of LSTs

The LST data can be derived from the TIR band of the Landsat images. So far, there are several well-documented methods for the retrieval of LST values from at-sensor and auxiliary data, including a single-channel algorithm (Jimenez-Munoz, Sobrino 2003) and a mono-window algorithm (Qin *et al.* 2001). However, their applications are limited due to the limited availability of the atmospheric parameters required by these algorithms (Li *et al.* 2012). Therefore, the image-based method, which has been successfully applied to retrieve LST data in previous studies, is used in this study because it does not require atmospheric parameters.

By adopting the Plank function (Eq. (2)), the spectral radiance was further converted into the brightness temperature (Chander *et al.* 2009):

$$T_B = \frac{K_2}{\ln\left(1 + \frac{K_1}{L_\lambda}\right)}, \quad (2)$$

where  $T_B$  represents the brightness temperature in Kelvin, and  $L_\lambda$  means the spectral radiance at the satellite's aperture.  $K_1$  and  $K_2$  mean the calibration constants, which are listed in Table 1.

Table 1. The calibration constants for Landsat images.

	$K_1$ (W/(m <sup>2</sup> ×sr×μm))	$K_2$ (K)
Landsat 7 ETM+	666.09	1282.71
Landsat 8 TIRS 10	774.89	1321.08

The brightness temperature is calculated with reference to a black body. Therefore, corrections of their spectral emissivities need to be conducted. The emissivity-corrected LST was generated using Eq. (3) (Artis, Carnahan 1982):

$$LST = \frac{T_B}{1 + \left(\lambda + \frac{T_B}{\rho}\right) \times \ln \varepsilon}, \quad (3)$$

where  $\rho = h \times c / \sigma$  ( $1.438 \times 10^{-2}$  mK),  $h$  is the Planck's constant ( $6.626 \times 10^{-34}$  Js),  $c$  is the velocity of light ( $2.998 \times 10^8$  m/s),  $\sigma$  is the Boltzmann constant ( $1.38 \times 10^{-23}$  J/K),  $T_B$  represents the brightness temperature value, and  $\lambda$  represents the wavelength of emitted radiance (11.5 μm) (Markham,

Barker 1985).  $\varepsilon$  means the land surface emissivity, which was calculated using NDVI threshold method proposed by Sobrino *et al.* (2004):

$$\varepsilon = \varepsilon_{soil} \quad (NDVI < 0.2); \quad (4)$$

$$\varepsilon = \varepsilon_{veg} \quad (NDVI > 0.5); \quad (5)$$

$$\varepsilon = \varepsilon_{veg} \times P_v + \varepsilon_{soil} \times (1 - P_v) \quad (0.2 < NDVI < 0.5), \quad (6)$$

where  $\varepsilon_{soil}$  and  $\varepsilon_{veg}$  represent the soil emissivity and vegetation emissivity, respectively. Soil and vegetation emissivity are estimated to be 0.97 and 0.99, respectively (Li *et al.* 2004).  $P_v$  represents the vegetation proportion based on NDVI (Carlson, Ripley 1997):

$$LST = \left( \frac{NDVI - NDVI_{min}}{NDVI_{max} - NDVI_{min}} \right)^2, \quad (7)$$

where  $NDVI_{max} = 0.5$ ,  $NDVI_{min} = 0.2$ .

NDVI was calculated from the pixel value of the Landsat images using the Eq. (8):

$$NDVI = \frac{\rho(NIR) - \rho(RED)}{\rho(NIR) + \rho(RED)}, \quad (8)$$

where  $\rho(NIR)$  and  $\rho(RED)$  represent the reflectance values in the NIR and RED bands, respectively. These values were calculated using the following equation (Chander, Markham 2003):

$$\rho_\lambda = \frac{\pi \times L_\lambda \times d^2}{ESUN_\lambda \times \cos \theta}, \quad (9)$$

where  $\rho_\lambda$  is the planetary reflectance value,  $L_\lambda$  represents spectral radiance at sensor's aperture.  $ESUN_\lambda$  is the mean exoatmospheric solar irradiance in W/(m<sup>2</sup>μm),  $\theta$  is the solar angle at zenith,  $d$  represents the earth-sun distance in astronomical units.

### 2.3. Measures of the spatial pattern

Spatial metrics are commonly used to quantify the spatial patterns of individual patches, of patches belonging to a specific class, and of an entire landscape consisting of all types of patches. To describe and analyze spatial patterns, three class-level spatial metrics, which are sensitive to changes in landscape composition and spatial configuration, were calculated using Fragstats 4 (McGarigal *et al.* 2012). The selection of the metrics was based on the research objective and their values in representing specific spatial characteristics as already explored in previous studies on urban areas (Herold *et al.* 2005; Luck, Wu 2002; Schwarz 2010). Table 2 provides a description of the spatial metrics used in this study.

One of the most important issues in spatial metrics is defining the spatial extent of the study, as the extent directly affects the spatial metrics. The spatial domain refers to the geographic extent of the analysis. This study adopted block-based subdivisions for the metric calculations

examining the relationship between the urban spatial patterns and LSTs. The study area was divided into several subregions. The square block used in this study is the most commonly used shape in the field of spatial pattern analysis (Luck, Wu 2002; Weng 2007). The study area was first divided into several square blocks, 2×2 km, 3×3 km, and 4×4 km. A block size of 1 km could lead to the situation that no urban patch or only a few urban patches exist in some blocks, which generates noise in the spatial pattern analysis. Therefore, the study area was firstly divided into several square blocks of 2×2 km. The selected metrics (PLAND, PD, and SHAPE\_MN) were then calculated for every block. A statistical relationship can be explored using each block as a data point.

Table 2. Description of the spatial metrics used in this study.

Spatial metrics	Abbreviation	Description
Percent of landscape	PLAND	PLAND is the areas (m <sup>2</sup> ) of all patches belonging to the same type, divided by the total landscape area (m <sup>2</sup> ) and multiplied by 100.
Patch density	PD	PD is the patches number in the landscape, divided by the landscape area (m <sup>2</sup> ), and multiplied by 10,000 and 100.
Mean shape index	SHAPE_MN	SHAPE index describes the complexity of a patch shape. This index is set to one when the patch has a square shape and increases as the irregularity of the shape increases. SHAPE_MN is the sum of the shape index of the patches, divided by the number of patches of the same type.

## 2.4. Statistical analysis

Regression models were applied to quantify the effects of the urban spatial pattern on LSTs. In contrast to OLS, a geographically weighted regression (GWR) is conducted using localized points to investigate the spatially varying relationships between explanatory variables and LST. Thus, instead of producing a global parameter for each relationship, GWR can estimate a set of local parameters that can be mapped for insight into hidden possible causal mechanisms. In other words, GWR can be used to investigate the spatially varying relationships between urban spatial patterns and LSTs by generating a set of local parameter estimates (Brunsdon *et al.* 1996; Fotheringham *et al.* 1996; Li *et al.* 2014). Moreover, the GWR model results are mappable and can be combined with GIS, which offers a powerful tool for analyzing spatially dependent relationships (Tu 2011).

The GWR model can be expressed as follows:

$$y_i = a_0(\mu_i, \nu_i) + \sum_k a_k(\mu_i, \nu_i)x_{ik} + \varepsilon_i, \quad (10)$$

where  $(\mu_i, \nu_i)$  is the coordinate location of the *i*th point.  $a_0$

$(\mu_i, \nu_i)$  and  $\alpha_k(\mu_i, \nu_i)$  are the intercept and local parameter estimate for independent variable  $x_{ik}$  at location *i* respectively.  $\varepsilon_i$  represents the random error term at location *i*.

In GWR, parameters for each observation at location *i* can be estimated by weighting all observations around a specific point *i* according to their spatial proximity, which is calculated as the Euclidean distance in this study. Observations that are spatially closer to location *i* will have a greater impact on its local parameter estimates than those from more distant points. A Gaussian distance-decay can be used to express the weighting function:

$$w_{ij} = \exp\left(-\frac{d_{ij}^2}{h^2}\right), \quad (11)$$

where  $w_{ij}$  is the weight of observation *j* for location *i*.  $d_{ij}$  is the Euclidean distance between points *i* and *j*. *h* represents a kernel bandwidth that affects the distance-decay of the weighting function.

The results generated from GWR are sensitive to bandwidth (Gao, Li 2011). Therefore, it is necessary to identify the optimum bandwidth when estimating the model. There are three choices of bandwidth methods: the corrected Akaike information criterion (AICc), cross validation and bandwidth parameter. If the bandwidth is known a priori, the bandwidth parameter can be applied. If it is unknown, the former two types use an automatic method to find the optimum bandwidth. In this study, the AICc method was used with the GWR model. The AICc method finds the bandwidth that minimizes the AICc value. Models with lower AICc values suggest a higher likelihood of the regression model reflecting reality.

For comparison purposes, OLS models were also employed to investigate the relationships between the urban spatial patterns and LSTs. To compare the performances of these two models (GWR and OLS), three statistical parameters were used: the adjusted R<sup>2</sup>, AICc, and Moran's I. The adjusted R<sup>2</sup> and AICc values provide some indications of the goodness of fit of the corresponding model. A higher adjusted R<sup>2</sup> value indicates that more variances can be explained for the dependent variable. Moran's I is an indicator of spatial autocorrelation ranging from -1 to 1. The larger the value of the Moran's I, the more significant the spatial autocorrelation. Residuals are defined as the differences between predicted and observed values. The Moran's I value was employed to investigate the spatial autocorrelations based on the residuals, and thus the models abilities to address the spatial autocorrelations can be evaluated and compared.

## 3. Results

### 3.1. Land cover dynamics

The multitemporal land-cover classification maps for Hangzhou City are shown in Figure 2. The overall classification accuracies calculated for 2002 and 2013 were 86% and 90%, respectively. The urban expansion in Hangzhou was focused on the development of new built-up land, as

well as in the expansion of the existing city core. To promote regional economic integration, polycentric development has been proposed to guide the future development of Hangzhou.

The individual class areas are presented in Table 3. As an overall trend, intense land-cover changes in Hangzhou City was characterized by a dramatic growth in built-up land and a gradual reduction in farmland and vegetation. The area of built-up land, which had the largest growth of all land-cover types, increased from 305.40 km<sup>2</sup> in 2002 to 1002.35 km<sup>2</sup> in 2013. It suggests that Hangzhou City experienced rapid urban growth processes over the study period. The great pressure of rapid urban growth on non-urban land was reflected by the reduction in farmland and vegetation area. The farmland and forest decreased by 482.87 km<sup>2</sup> and 127.3 km<sup>2</sup>, respectively.

Table 4 indicates that a total of 696.95 km<sup>2</sup> of land was converted into built-up land, accounting for approximately 67.0% of the total land-cover change area during 2002–2013. As indicated, the majority of the additional built-up land came from the conversion of farmland for

urban uses. In particular, 89.3% of the increase in built-up land was due to converted farmland during the period of 2002–2013. This change reflects the conflict between the increasing demand for built-up land and the limited land resources of the city.

### 3.2. Spatial distribution of LST

The two Landsat images were taken in the mid-summer. Figure 3 shows the spatiotemporal distribution of the LSTs in Hangzhou City. A clear temperature gradient was observed in each LST image. Across the study area, LST values decreased gradually from the central urban area to the rural areas. The UHI was extensively distributed in the built-up area, while cold spots were distributed in the western region, which was covered by forest and farmland. Furthermore, the results also present a continuously increasing extent of areas with higher LST values during the study period.

In 2002, the areas with higher LST values were mainly located in the city core and some of its major centers, with

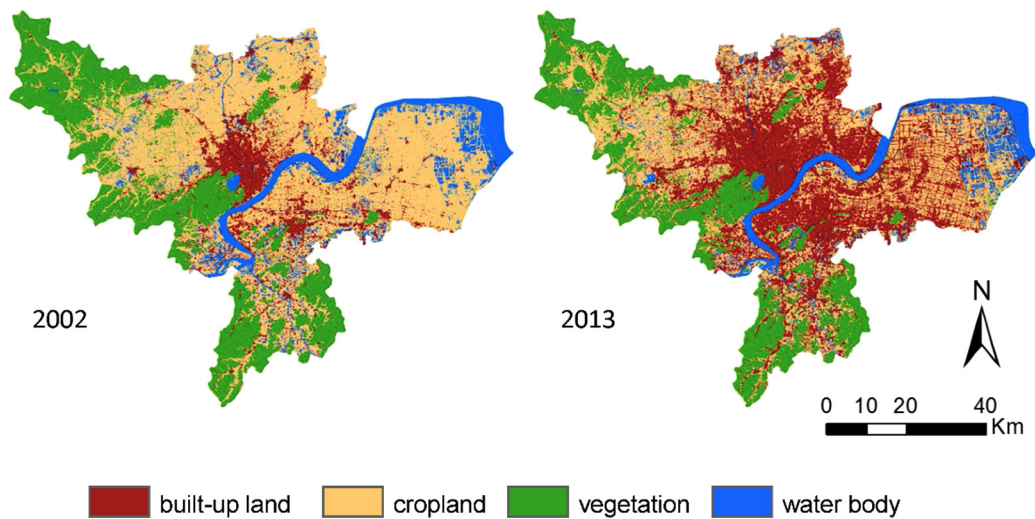


Figure 2. Classified land cover maps of Hangzhou city in 2002 and 2013

Table 3. Land cover statistical data of Hangzhou city

	Built-up		Farmland		Forest		Water body	
	Area (km <sup>2</sup> )	Percent (%)						
2002	305.4	9.09	1792.88	53.38	868.76	25.87	391.63	11.66
2013	1002.35	29.84	1310.01	39.00	741.46	22.08	304.84	9.08

Table 4. Matrices of land cover changes in Hangzhou city from 2002 to 2013 (unit: km<sup>2</sup>)

		Built-up	Farmland	Forest	Water body
		2002			
2013	Built-up	305.4	622.68	17.90	56.36
	Farmland	0.00	1071.15	149.14	89.72
	Vegetation	0.00	40.08	699.18	2.20
	Water body	0.00	58.97	2.54	243.34

a typical strip-shaped related to the roads. Outside the city core, the areas with higher LSTs were mainly located in industrial parks, which are characterized by intensive traditional industries. Compared to the LST map of Hangzhou in 2002, the extent of the areas with higher LST values in 2013 increased dramatically, accompanying the rapid urbanization. The span of the UHI expanded outward from the city core to the fringe areas as the main urban area grew. Due to the implementation of the developmental strategy of “great-leap-forward development along the Qiantang River”, rapidly developed infrastructures, industrial parks, and other built-up land emerged along the Qiantang River, leading to the southward and eastward expansion of the built-up regions. The closer link between the city core and small connected regions resulted in the significant development of these areas. This development strategy may help to explain the observed change in the LST patterns. Note that some cold spots, although small, exist within the city core and newly developed regions with higher LST values. This could be attributed to the public green space restructuring policy. Some new green space patches, such as forest parks and urban parks, were developed in order to create a better living environment. In addition, the magnitude of the LST values between the UHI and other areas varied remarkably, depending on the different years and their land-cover types.

The summarized characteristics of the LSTs on the two dates used in this study are shown in Table 5. The average LST value increased from 28.15 °C in 2002 to 30.20 °C in 2013. The standard deviation of the LSTs in 2013 was higher than that of the LSTs in 2002, suggesting higher

Table 5. Descriptive statistics of LST (unit: °C)

	Max	Min	Mean	Std dev
2002	39.09	23.88	28.15	1.64
2013	45.27	14.24	30.20	3.32

variations of LSTs in 2013. Although the minimum temperature value decreased over the study period, the maximum value increased dramatically.

Distinctive LST patterns are related to the thermal characteristics of the individual land-cover types. To better understand the effects of the land-cover types on LSTs, the LST values of each land-cover type were acquired by overlaying an LST image with a land-cover map of the same date. The mean and standard deviation values of the LSTs for the different land-cover types are summarized in Table 6. Note that the built-up area exhibited the highest average LST values, followed by those of the farmlands, but the lowest average temperature was recorded in the forest area. All the built-up areas had relatively high temperatures. The differences in the LST patterns over the study period reflect the impacts of land-cover changes on thermal environments. The different impacts of varying landscape compositions on LSTs can be attributed to the fact that each land-cover type exhibits unique thermal, radiation, and moisture characteristics (Oke 1982). Given the growing extents and magnitudes of hot spots during the study period, rapid urbanization and land-cover changes intensified the UHI effect in the rapidly developing region. As shown in the results, the variations of the vegetation cover and built-up areas have significant effects on the thermal conditions of cities and the formation of UHIs.

Table 6. Average LST associated with land cover types (unit: °C)

	LST2002		LST2013	
	Mean	Std dev	Mean	Std dev
Built-up	31.41	1.21	33.82	1.98
Cropland	28.42	1.37	29.79	2.17
Vegetation	26.79	1.26	27.18	2.03
Water body	27.34	1.43	27.14	2.15

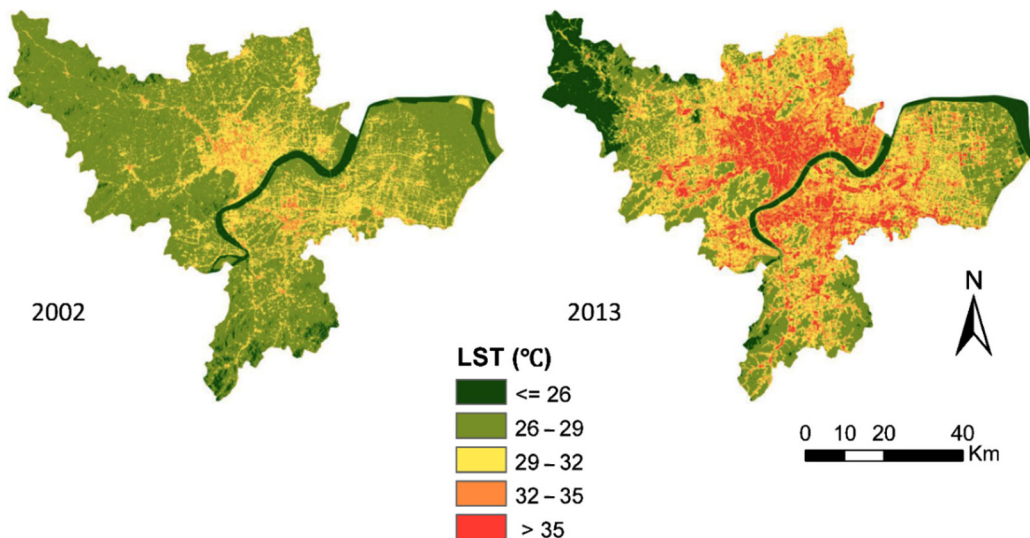


Figure 3. Spatial pattern of LST derived from Landsat images

### 3.3. Effects of urban spatial patterns on LST

To correlate the LSTs with the spatial metrics, the mean LST values and spatial metrics were calculated for each 2×2 km, 3×3 km, and 4×4 km block.

As shown in Figure 4, the LST values and the selected spatial metrics varied significantly across spatial scales. The maximum value of the LST in 2002 was 35.45 °C when using 2-km blocks but was 33.59 °C and 33.05 °C when using the 3-km and 4-km blocks, respectively. In contrast, the maximum temperature in 2013 increased with increasing block size. However, the mean temperature still increased at all spatial scales from 2002 to 2013. This could be due to the expansion of the UHI. As demonstrated by the results, the mean values of PLAND and PD dramatically increased with the continued urbanization process, which is consistent with the land-cover change analysis. Additionally, the maximum PLAND, PD, and SHAPE\_MN declined with increased block sizes. The larger blocks could inadvertently cover non-urban land in addition to urban land, which could cause the observed decrease in the metric values as the total block area increased.

Urban patterns are not only an indicator of urban development but also a contributor to the impacts of urban development (Arnold, Gibbons 1996). Therefore, it is important to analyze the relationship between urban spatial patterns and LSTs. Pearson correlation analysis (Table 7) shows that all of the spatial metrics were significantly related to the LSTs. However, according to the correlation coefficients, none of the spatial metrics had consistent correlations with the LSTs across spatial scales and time. The relationships between the LSTs and urban spatial metrics were stronger at finer spatial scales because the finer blocks retain more of the details of the spatial patterns. Further, the selected urban spatial metrics have stronger relationships with the LSTs in 2013. The dramatic

land-cover change resulted in fundamental changes of the urban spatial pattern since 2002, which significantly affected the variations of the LSTs.

PLAND is positively correlated with LST. In other words, LST increased with increase in the proportion of urban land cover. This could be explained by the fact that impervious surfaces can increase the LST through changes in the evapotranspiration process (Yuan, Bauer 2007). High LSTs were usually observed in urban areas with high patch densities. In addition, the LST had a positive relationship with the mean patch shape index. Urban areas with complex patch shapes tended to have high LSTs. Furthermore, the correlation coefficient of SHAPE\_MN varied from 0.323 to 0.491 between 2002 and 2013, which implies that the effects of the urban patch shapes became stronger over time. Pearson correlation analysis results also show that the effect of SHAPE\_MN on LSTs was not as strong as the effects of the other two spatial metrics, although there is a heating effect associated with an increase in the mean urban patch shape index. The coefficients of SHAPE\_MN at the 4-km scale are statistically significantly correlated with energy consumption at the 95% confidence level in 2002.

Table 7. Pearson correlation between LST and spatial metrics

		PLAND	PD	SHAPE_MN
2km	2002	0.590**	0.402**	0.323**
	2013	0.775**	0.569**	0.491**
3km	2002	0.548**	0.366**	0.287**
	2013	0.723**	0.564**	0.463**
4km	2002	0.444**	0.356**	0.142*
	2013	0.640**	0.516**	0.416**

Note: \*\* Correlation is significant at the 0.01 level (2-tailed).

\* Correlation is significant at the 0.05 level (2-tailed).

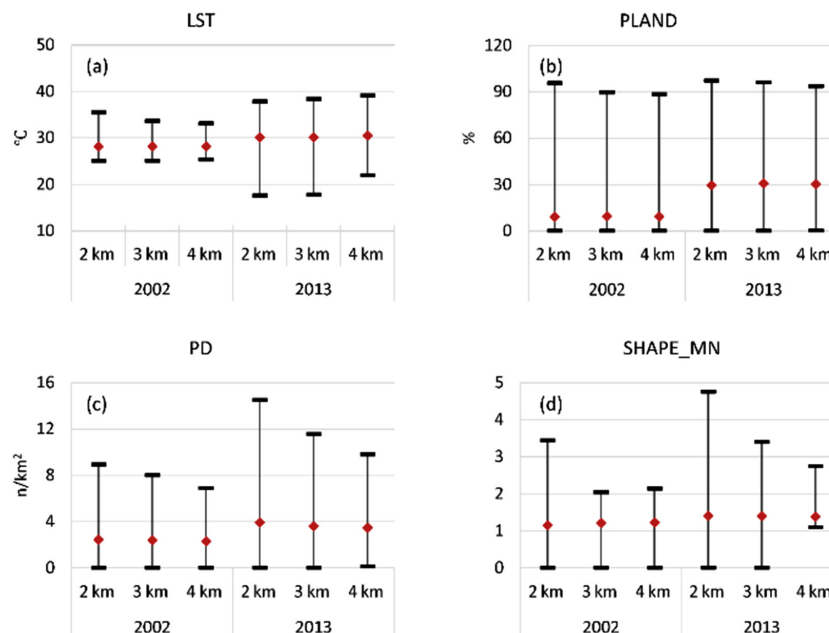


Figure 4. Maximum, minimum and mean value of variables at different spatial scales

In addition to Pearson correlation analysis, OLS and GWR were also used in this study. The OLS model uses the entire region to investigate the impacts of the urban spatial patterns on LSTs. The results provide only a single statistical average parameter for the whole area; in contrast, the GWR results suggest the variable changes throughout the study area. The adjusted  $R^2$  and AICc values generated by the GWR and OLS models for the different periods are shown in Tables 8–9. In all cases, the results obtained by GWR are characterized by higher adjusted  $R^2$  and lower AICc values than those of the corresponding OLS models. The adjusted  $R^2$  values of GWR ranged from 0.462 to 0.740 at the 2-km scale, which are considerably higher than those of the corresponding OLS. This indicates that more than 46.2% of the variations in LSTs can be explained by the selected spatial metrics at the 2 km GWR model. However, this value declines for spatial scales coarser than 2 km. The

comparison of these two indicators suggests that the GWR models perform better than OLS models for investigating the relationships between LSTs and urban spatial patterns. The GWR model explained more of the variance in the LSTs than the OLS model did. The results generated from GWR indicate that the variations of LST are significantly associated with urban spatial patterns.

Moreover, Table 10 also summarizes the Moran's I values of the model residuals from both the GWR and OLS models. The higher Moran's I values ranging from 0.103 to 0.563 indicates the significant positive spatial autocorrelations in all the OLS models. In contrast, the Moran's I values of the GWR models are lower than 0.100, which indicates that the spatial autocorrelation can be better simulated by the GWR models.

Urban spatial patterns exhibit different characteristics, depending on the scale of the observations and analyses

Table 8. Comparison of coefficient of determination (adjusted  $R^2$ ) between GWR and OLS

		2002			2013		
		PLAND	PD	SHAPE_MN	PLAND	PD	SHAPE_MN
2 km	Adjusted $R^2$ G	0.537	0.483	0.462	0.740	0.657	0.622
	Adjusted $R^2$ O	0.348	0.128	0.104	0.257	0.001	0.241
3 km	Adjusted $R^2$ G	0.447	0.436	0.363	0.664	0.598	0.505
	Adjusted $R^2$ O	0.301	0.162	0.082	0.223	0.005	0.214
4 km	Adjusted $R^2$ G	0.287	0.349	0.136	0.585	0.566	0.387
	Adjusted $R^2$ O	0.197	0.120	0.020	0.109	0.002	0.173

Note:  $R^2$ G is the  $R^2$  for GWR model;  $R^2$ O is the  $R^2$  for OLS model.

Table 9. Comparison of AICc between GWR and OLS

		2002			2013		
		PLAND	PD	SHAPE_MN	PLAND	PD	SHAPE_MN
2 km	AICcG	2607.509	2757.304	2802.591	3464.309	3781.822	3822.441
	AICcO	2793.155	3038.310	3061.106	3674.442	4448.771	4216.959
3 km	AICcG	1199.726	1239.802	1255.225	1526.892	1596.883	1633.077
	AICcO	1247.119	1311.482	1343.676	1598.606	1860.362	1776.275
4 km	AICcG	699.839	711.256	734.052	942.571	970.917	991.849
	AICcO	708.508	727.100	749.009	967.525	1073.963	1035.917

Note: AICcG is the AICc for GWR model; AICcO is the AICc for OLS model.

Table 10. Comparison of Moran's I of the residuals from GWR and OLS

		2002			2013		
		PLAND	PD	SHAPE_MN	PLAND	PD	SHAPE_MN
2 km	Moran's IG	0.019	0.007	0.009	0.005	0.003	0.046
	Moran's IO	0.147	0.103	0.132	0.107	0.389	0.227
3 km	Moran's IG	0.027	0.034	0.026	0.012	0.010	0.072
	Moran's IO	0.160	0.260	0.260	0.229	0.507	0.316
4 km	Moran's IG	0.035	0.091	0.041	0.085	0.084	0.098
	Moran's IO	0.206	0.293	0.288	0.280	0.563	0.356

Note: Moran's IG is the Moran's I for GWR model; Moran's IO is the Moran's I for OLS model.

(Wu *et al.* 2002). The variations of the adjusted  $R^2$ , AICc, and Moran's I over the different block scales showed these characteristic differences. As the block scales increased, the adjusted  $R^2$  values decreased. The adjusted  $R^2$  values of the GWR and OLS models at the 3 km and 4 km scales were generally lower than those at the 2-km scale. Thus, the 2 km GWR models are better able to explain the relationships between urban spatial patterns and LSTs. Moreover, the Moran's I values were higher at 3 km and 4 km scales than at the 2-km scale.

The spatial patterns of the coefficients estimated by the GWR model are shown in Figures 5–7. As indicated by the results, the spatially varying coefficients show spatial variations of the relationships between the three spatial metrics and LSTs across the study area. Thus, the homogeneities and heterogeneities in the relationships between the LSTs and spatial metrics were sensitive to the spatial scales analyzed.

Though the magnitude of the correlations varied across the study area, a positive relationship between PLAND and LST was consistently observed. At the finest spatial scale (2 km), PLAND can explain 53.7% and 74.0% of the variations in the LSTs of 2002 and 2013, respectively. In 2002, a significant positive correlation coefficient smaller than 0.10 is observed for a large part of Hangzhou City, implying that accelerating urbanization could result in an increase in LST. This is consistent with several previous studies, which demonstrated positive correlations between LSTs and the abundance of urban areas, as well as negative correlations between LSTs and the abundance of green spaces. Green space can lower surface temperature because of the modification of the land surface characteristics such as evapotranspiration and albedo (Hamada, Ohta 2010; Zhou *et al.* 2011). The temporal variation in the effects of urban expansions were also investigated in this study. Along with urbanization processes, the magnitude of the effects of PLAND on the LSTs increased. The variations in LSTs in the fringe areas showed strong effects from the urban expansion.

The correlations between PD and LST are shown in Figure 6. Importantly, the coefficients of the explanatory variables took positive or negative values according to their spatial locations. For both observed dates, the PD had a significant negative impact on the LSTs in the city core, as evidenced by coefficients lower than 0.0. This indicates that decreasing patch densities could lead to increased LSTs. The continuous expansions of the existing urban patches in the city core lead to decreased patch densities. Some individual urban patches continued to grow together to form larger patches. Decreases in patch density may increase LSTs because larger, continuous urban areas produce stronger UHI effects than those from several small pieces of urban areas. In the fringe area, however, the PD was positively related to the LSTs. In 2013, the area with negative coefficients is larger than that in 2002. In the fringe areas, the estimated coefficients changed from positive to negative. The massive constructions of infrastructure and factories connected many isolated urban patches

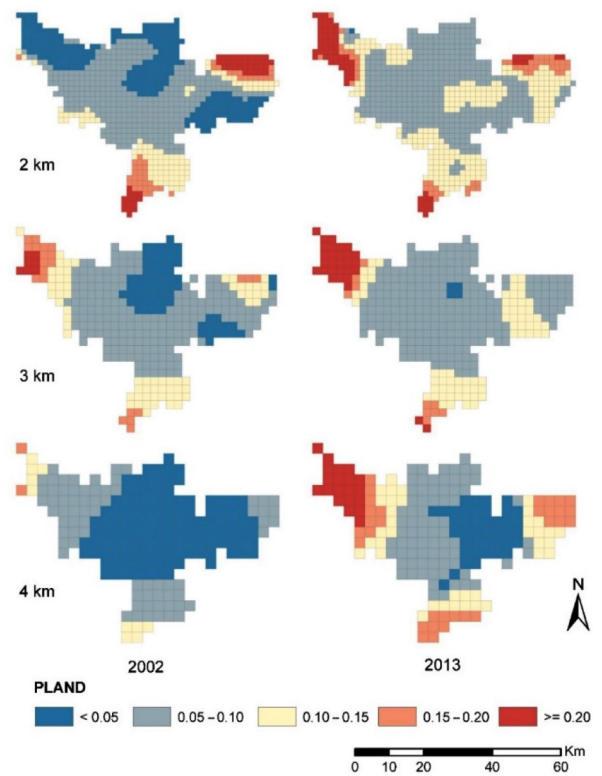


Figure 5. Spatial distributions of the correlation coefficients obtained from GWR for PLAND at three scales (2 km, 3 km, and 4 km)

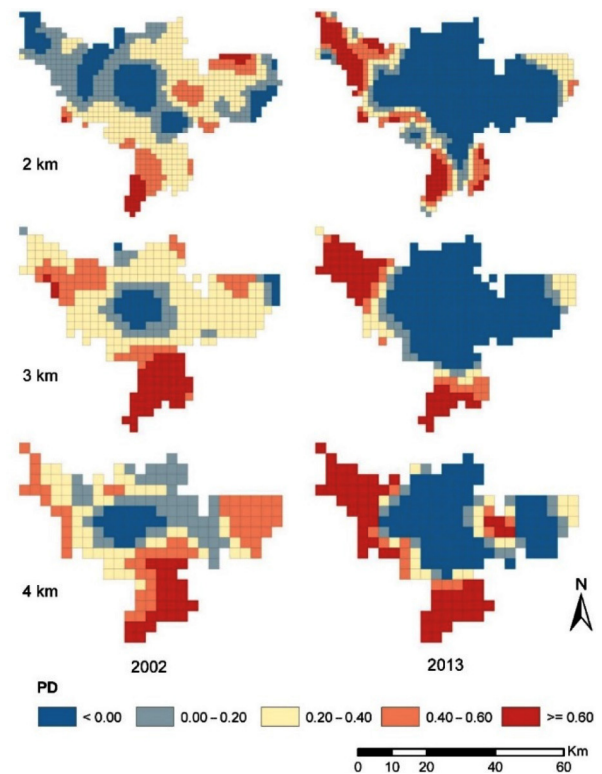


Figure 6. Spatial distributions of the correlation coefficients obtained from GWR for PD at three scales (2 km, 3 km, and 4 km)

in fringe areas, which has been a key factor in the rapid expansion of urban areas. Therefore, the decrease in PD is accompanied with the increase in urban land, which can be used to explain the negative effects of PD on LST. The results suggest that fragmented urban areas are better than aggregated urban area for decreasing LSTs in intensive urbanization area. The relationship between LST and PD of urban land, however, is not consistent. LST is positively correlated with PD in less urbanized area.

The mean urban patch shape index significantly affects the magnitude of the LSTs. As shown in Figure 7, the spatial patterns of the coefficients of variable SHAPE\_MN exhibit significant regional and temporal variations. In 2002, there were strong positive trends closer to the city core. In other words, an increase in the SHAPE\_MN around the city core is significantly associated with an increase in LST. Increasing the SHAPE\_MN values around the city core by one results in an at least 2 °C increase in LSTs. Notably, the relationship between SHAPE\_MN and LST is stronger in 2013 than that in 2002. During the period of 2002–2013, Hangzhou experienced rapid urbanization. The potential for further urbanization in the city center was exhausted after this rapid development. Therefore, the vacant land in the fringe areas received more attention. As such, a strong relationship, with the coefficient values larger than 2.0, was identified between the LSTs and SHAPE\_MN values in the fringe area in 2013, which indicates that increasing the irregularities and complexities of urban patches could cause higher LSTs in fringe areas than those produced in other

areas. The positive correlation coefficient of SHAPE\_MN indicates that LST increases when urban patches are more irregular. The expanded urban areas in the fringe areas are always highly irregular in shape. As a new development area, the fringe area of Hangzhou City experienced a significant increase in SHAPE\_MN with its urbanization, which could result in a strong relationships between LSTs and SHAPE\_MN values in the fringe areas.

The effects of the different scales cannot be underestimated when analyzing the relationships between different variables. The variational trends of the coefficients for three spatial metrics exhibited significant scale dependence, which implies that the effects of the spatial patterns of these coefficients on LSTs vary have a similar scale dependence. Specifically, the area where PLAND has slight effects on LST became larger as the scale increased. A larger area showing the positive effect of PD on LST can be identified when using the scale of 4 km. Although similar changes of the effects of SHAPE\_MN on LST were found at different scales, the strong relationship of LST with SHAPE\_MN was found for a larger areas at larger scales.

## 4. Discussion

### 4.1. Effects of urban spatial patterns on LST

The results indicate that the abundance of urban land plays a more important role in influencing LST values than the fragmentation and irregularity of urban land, which is consistent with previous studies (Zhou *et al.* 2011). Decreasing the area of urban land could significantly decrease LST, likely because changing the urban land area could result in variations of land surface characteristics. An increase in urban land is also positively related to the rising production of waste heat from refrigeration systems, air conditioners and vehicular traffic, all of which could intensify the UHI effect.

Unlike previous studies, which only analyzed the composition indicators related to land cover and the abundance indicators, a set of spatial metrics were applied in this study to describe the detailed urban spatial patterns. Modifying the fragmentation and irregularity of a fixed urban land area is also an effective way to mitigate UHI effects, since varying spatial configurations affect the flow of energy and the energy exchange (Forman 1995).

However, previous studies have demonstrated that the relationship between LST and land cover spatial patterns is not consistent. LST is negatively correlated with patch density in Shanghai (Li *et al.* 2011), but a positive relationship between them was reported in Beijing (Li *et al.* 2012). The different effects of spatial patterns on LSTs could be attributed to regional difference among different cities. In addition to the regional differences, our study investigates the spatiotemporally varying effects of urban spatial patterns instead of just the global effects. The magnitude of the effects of urban spatial patterns on LSTs appear complicated within Hangzhou City. LST increases with a decrease in PD in the city core in 2002. In the fringe areas,

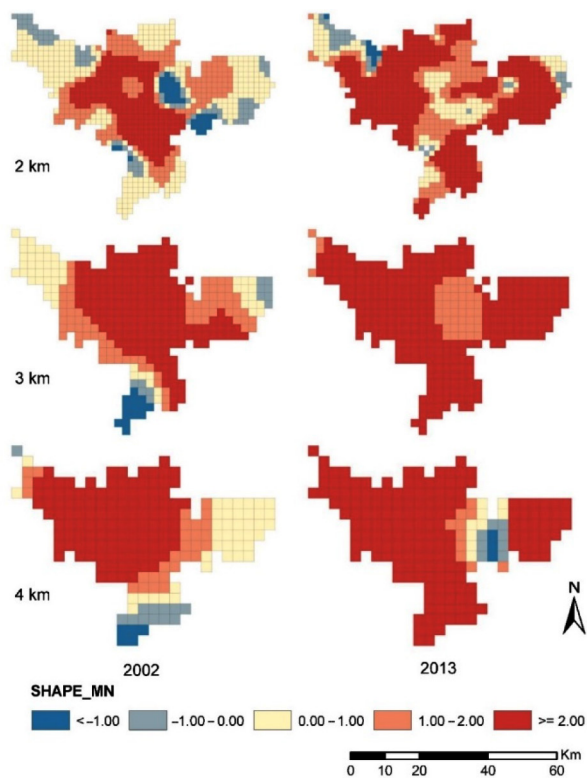


Figure 7. Spatial distributions of the correlation coefficients obtained from GWR for SHAPE\_MN at three scales (2 km, 3 km, and 4 km)

an increase in PD could lead to an increase in LST. In 2013, however, a negative effect of PD was found in the fringe area. The increase in the shape complexity of the urban patch in the city core led to a dramatic increase in LST in 2002. In contrast to the situation in 2002, a dramatic increase in LST caused by the increase in patch shape complexity was found in the fringe and rural areas in 2013. The positive correlation between SHAPE\_MN and LST could be because an increase in shape complexity may increase the solar heat gain due to an increased exposed surface (Voogt, Oke 1998).

The spatiotemporally varying relationship between LST and urban spatial patterns also demonstrated urban growth processes in rapid urbanization areas, such that the urban land expanded from the city core to the fringe and rural areas (Dewan, Yamaguchi 2009; Pham *et al.* 2011). The expansion of new urban lands tended to be clustered around the city core, while new developments in open areas were rather scarce. Afterward, a larger proportion of urban expansion in Hangzhou was focused on the development of new urban patches in the fringe and rural areas, rather than on the expansion of the existing urban patches in the city core. As the new planning policy, polycentric development policy has been implemented to guide the future development of Hangzhou. The newly developed areas in the fringe and rural areas can be used to improve the infrastructures and facility conditions during further developments.

#### 4.2. Methodology implication

Our study indicates that the integration of remote sensing, spatial metrics, and spatial models is effective for monitoring LST and analyzing the effects of urban spatial patterns on LST.

PLAND, PD, and SHAPE\_MN were used in this study, thus focusing this work on three aspects of urban spatial patterns: the abundance of urban land, its fragmentation and its irregularity. These spatial metrics were calculated based on blocks, making it possible to discover and locate patterns in different locations. Moreover, the local scale allowed us to better evaluate small-scale urbanization processes, which cannot be detected at the global scale.

Choosing an appropriate model is important to understand the relationship between urban spatial pattern and LST. However, many studies examined these pattern-process relationships using traditional regression models, which estimated the global relationship over the entire study area (Batisani, Yarnal 2009; Weng 2007). Consequently, any spatially varying effects of the driving factors on the urban spatial patterns are lost.

One of the crucial findings in the study is the use of the GWR model, which enables analysis of the spatial variability of the results. The result indicates that the coefficients vary by geographical location. The results show that GWR models can provide better insight into the different roles of urban spatial patterns in different locations rather than generating an average coefficient for the entire area.

This regionality can provide an improved explanation of the local variations of LSTs. The comparison of the GWR and OLS models suggests that the GWR models perform better than the OLS models in explaining the variances of the urban spatial pattern and LST relationship. It has been widely acknowledged that LST is spatially autocorrelated to or dependent on the land surface heat fluxes (Song *et al.* 2014). The spatial autocorrelation of LST suggests that the LST value at a specific location is correlated with those of its neighboring locations. Therefore, using traditional regression models without considering the autocorrelation of the spatial variable can cause misleading results. GWR models improve the reliability of these relationships by effectively addressing spatial autocorrelations. Therefore, the GWR model is useful for establishing effective urban plans towards mitigating the UHI effects by reducing the LST values.

One of the differences from previous studies is that this work shows a combined analysis of spatiotemporal changes of the relationships between urban spatial patterns and LSTs. This study added a temporal dimension to the GWR model. The result reveals not only how the relationships change spatially over the study area but also when the relationships change temporally in response to urbanization. The temporal changes of the effects of the urban spatial patterns on LSTs is missing in traditional analyses.

It has been widely recognized that urban spatial patterns are dependent on the scale of observation and analysis (Wu *et al.* 2002). Much attention has been paid to analyzing the spatial scales in remote sensing and landscape ecology. However, one important problem that has been often ignored by previous studies, which is the scale effects on the relationship between LSTs and urban spatial patterns. After all, the analysis of the relationship between LSTs and urban spatial patterns has usually been conducted at only one scale (Maimaitiyiming *et al.* 2014; Zhou *et al.* 2011). This study extends these previous studies by examining their relationships at multiple scales.

The findings provide the specific examples of the effects of different spatial scales. It indicates that the LST values and spatial metrics varied significantly across spatial scales. The advantage of GWR over OLS was demonstrated at all spatial scales since the former has larger adjusted  $R^2$ , lower AICc and Moran's I values. Furthermore, the GWR model performs better at the 2-km scale when exploring the relationship between LSTs and urban spatial patterns than it does at other scales.

Spatial scales can lead to variations not only in the values of the dependent and independent variables but also in the relationships between these variables. Our findings generally agree with the reported findings, such that our results show that the relationships have different behaviors at various scales (Su *et al.* 2011). The relationship between LST and PLAND was positive across spatial scales. This is consistent with the well known positive relationship between LST and urban abundance (Bokaie *et al.* 2016). In

addition, the results demonstrate that the correlation coefficients change significantly as a result of the spatial scale effect. The correlation coefficients between the individual spatial metrics and LST decreased as the spatial scales increased. This indicates that, as the scale becomes coarser, the impact of the urban spatial pattern on LST becomes weaker. Furthermore, by combining the spatial scale analysis with the GWR model, this study examines how spatial scales influenced the relationship between LST and urban spatial patterns at different locations. For example, the total fringe areas with negative correlations between PD and LST decreased as the scale increased from 2 km to 4 km. Differing from the previous studies of the effects of scale on correlation magnitudes (Li *et al.* 2013), this study provides an improved understanding of the scaling effects on the spatially varied relationships between LST and urban spatial patterns. Hence, spatial scales should be treated as a factor that influences the magnitude of the UHI effect, and studies should address how the scale affects the relationships between spatial metrics and LSTs differentially across space and time.

### 4.3. Development implication

The continuous increase in LST associated with rapid urban development has negative effects both on the human population and the ecosystems within cities. This threat poses huge challenges for the city planners and decision makers attempting to implement a sustainable urban development strategy. The results of this study reveal that urban areas strongly influence LST. Appropriate planning, such as reducing urban land cover and creating vegetation cover in urban areas, should be designed and implemented in order to mitigate UHI effects. This corresponds with the findings in the literature related to other cities in the world (Bokaie *et al.* 2016; Li *et al.* 2013).

However, urbanization is a never-ending process. Fast economic growth and urbanization are currently the main goals of the Chinese government (Fang *et al.* 2015). The conflict between rapid urban development and limited land resources becomes more apparent in the rapidly developing cities in China. However, the reduction of the UHI effect must be maintained during rapid urbanization. Given this situation, the government faces the tremendous challenges in balancing the continual increase in the LSTs and rapid economic growth with environmental responsibility.

Importantly, the dynamics of the changes of urban spatial configurations underlying rapid urbanization have a significant impact on LST values. Even if we cannot decrease the percentage of urban areas in cities where the land resources are valuable and scarce, an optimization of urban spatial patterns through spatial planning and urban land use management can be an effective way to reduce the UHI effect while maintaining rapid economic growth.

Although significant effects of urban spatial patterns on LSTs were found in Hangzhou City, the effects of urban spatial patterns on LSTs varied spatiotemporally, which

can be explained by the different levels of urban development. The planners and managers should use a set of locally specific coefficients to investigate the impacts of spatial patterns on LSTs in their own local settings. The planning measures should not be the same within Hangzhou City. The design and implementation of the planning and land use management should consider the disparities of the regions within the study area in order to effectively mitigate UHI effects.

### 4.4. Outlook

The methodological framework proposed in this study has demonstrated its use in analyzing the relationship between the urban spatial patterns and LSTs in Hangzhou City and in providing support for decision making to mitigate UHI effects. The valuable results provide an insight into the spatiotemporal variations of LSTs and the effects of urban spatial patterns on LST. However, there are several limitations that need to be addressed by further studies.

Considering the relatively low spatial resolution of Landsat images, this study only generated urban land data without considering detailed land use classes, i.e., industrial, residential and commercial lands. However, the spatial distributions of the detailed land use categories are also important for analyzing the impacts of urban spatial patterns on LSTs (Zhou *et al.* 2011). It would be valuable to extract these land use categories using high-spatial-resolution remote sensing images and to examine the relationships between the spatial patterns of the detailed land use categories and LSTs. In addition, all LST data used in this study were obtained in the summer. Previous studies have proven that seasonal variations exist in the relationships between LSTs and urban spatial patterns (Buyantuyev, Wu 2010; Zhou *et al.* 2014). Therefore, it is necessary to conduct further studies using multiple LST datasets acquired in different seasons.

## Conclusions

In this paper, Landsat data were used to map and extract land cover information as well as LSTs in Hangzhou over the period of 2002–2013. In addition, the relationships between the urban spatial patterns and LSTs were explored using Pearson correlation analysis and GWR model. The results show that the LST patterns have changed significantly, which can be explained by the concurrent changes in urban spatial patterns. The correlation coefficients between the spatial metrics and LSTs decrease as the spatial scale increases. The GWR model performs better than an ordinary least squares analysis in exploring the relationship of LSTs and urban spatial patterns, which is indicated by the higher adjusted  $R^2$  values, lower corrected Akaike information criterion and reduced spatial autocorrelations. The GWR model results indicate that the effects of urban spatial patterns on LSTs are spatiotemporally variable. Moreover, their effects vary spatially with the use of different spatial scales.

## Funding

This work was supported by the Fundamental Research Funds for the Central Universities [grant number 2017QNB18].

## Disclosure statement

We declare that we do not have any competing financial, professional, or personal interests from other parties.

## References

- Akbari, H.; Pomerantz, M.; Taha, H. 2001. Cool surfaces and shade trees to reduce energy use and improve air quality in urban areas, *Solar Energy* 70: 295–310. [https://doi.org/10.1016/S0038-092X\(00\)00089-X](https://doi.org/10.1016/S0038-092X(00)00089-X)
- Arnold, C. L.; Gibbons, C. J. 1996. Impervious surface coverage: the emergence of a key environmental indicator, *Journal of the American Planning Association* 62(2): 243–258. <https://doi.org/10.1080/01944369608975688>
- Artis D. A.; Carnahan, W. H. 1982. Survey of emissivity variability in thermography of urban areas, *Remote Sensing of Environment* 12(4): 313–329. [https://doi.org/10.1016/0034-4257\(82\)90043-8](https://doi.org/10.1016/0034-4257(82)90043-8)
- Batisani, N.; Yarnal, B. 2009. Urban expansion in Centre country, Pennsylvania: spatial dynamics and landscape transformations, *Applied Geography* 29(2): 235–249. <https://doi.org/10.1016/j.apgeog.2008.08.007>
- Bokaie M.; Zarkesh, M. K.; Arasteh, P. D.; Hosseini, A. 2016. Assessment of Urban Heat Island based on the relationship between land surface temperature and Land Use/ Land Cover in Tehran, *Sustainable Cities and Society* 23: 94–104. <https://doi.org/10.1016/j.scs.2016.03.009>
- Brunsdon, C.; Fotheringham, A. S.; Charlton, M. 1996. Geographically weighted regression: a method for exploring non-stationarity, *Geographical Analysis* 28(4): 281–298. <https://doi.org/10.1111/j.1538-4632.1996.tb00936.x>
- Buyantuyev, V.; Wu, J. 2010. Urban heat islands and landscape heterogeneity: Linking spatiotemporal variations in surface temperatures to land-cover and socioeconomic patterns, *Landscape Ecology* 25(1): 17–33. <https://doi.org/10.1007/s10980-009-9402-4>
- Carlson, T. N.; Ripley, D. A. 1997. On the relation between NDVI fractional vegetation cover, and leaf area index, *Remote Sensing of Environment* 62: 241–252. [https://doi.org/10.1016/S0034-4257\(97\)00104-1](https://doi.org/10.1016/S0034-4257(97)00104-1)
- Chander, G.; Markham, B. L. 2003. Revised Landsat-5 TM radiometric calibration procedures and postcalibration dynamic ranges, *IEEE Transactions on Geoscience and Remote Sensing* 41(11): 2674–2677. <https://doi.org/10.1109/TGRS.2003.818464>
- Chander, G.; Markham, B. L.; Helder, D. L. 2009. Summary of current radiometric calibration coefficients for Landsat MSS, TM, ETM+, and EO-1 ALI sensors, *Remote Sensing of Environment* 113(5): 893–903. <https://doi.org/10.1016/j.rse.2009.01.007>
- Chavez, P. S. 1988. An improved dark-object subtraction technique for atmospheric scattering correction of multispectral data, *Remote Sensing of Environment* 24(3): 459–479. [https://doi.org/10.1016/0034-4257\(88\)90019-3](https://doi.org/10.1016/0034-4257(88)90019-3)
- Connors, J. P.; Galletti, C. S.; Chow, W. T. L. 2013. Landscape configuration and urban heat island effects: assessing the relationship between landscape characteristics and land surface temperature in Phoenix, Arizona, *Landscape Ecology* 28(2): 271–283. <https://doi.org/10.1007/s10980-012-9833-1>
- Dewan, A. M.; Yamaguchi, Y. 2009. Land use and land cover change in Greater Dhaka, Bangladesh: using remote sensing to promote sustainable urbanization, *Applied Geography* 29(3): 390–401. <https://doi.org/10.1016/j.apgeog.2008.12.005>
- Fang, C.; Wang, S.; Li, G. 2015. Changing urban forms and carbon dioxide emissions in China: a case study of 30 provincial capital cities, *Applied Energy* 158: 519–531. <https://doi.org/10.1016/j.apenergy.2015.08.095>
- Forman, R. T. T. 1995. *Land mosaics: the ecology of landscapes and regions*. Cambridge: Cambridge University Press.
- Fotheringham, A. S.; Charlton, M.; Brunsdon, C. 1996. The geography of parameter space: an investigation of spatial non-stationarity, *International Journal of Geographical Information System* 10(5): 605–627. <https://doi.org/10.1080/026937996137909>
- Gao, J.; Li, S. 2011. Detecting spatially non-stationary and scale-dependent relationships between urban landscape fragmentation and related factors using Geographically Weighted Regression, *Applied Geography* 31(1): 292–302. <https://doi.org/10.1016/j.apgeog.2010.06.003>
- Guo, G.; Zhou, X.; Wu, Z.; Xiao, R.; Chen, Y. 2016. Characterizing the impact of urban morphology heterogeneity on land surface temperature in Guangzhou, China, *Environmental Modelling & Software* 84: 427–439. <https://doi.org/10.1016/j.envsoft.2016.06.021>
- Gustafson, E. J. 1998. Quantifying landscape spatial pattern: what is the state of the art?, *Ecosystems* 1(2): 143–156. <https://doi.org/10.1007/s100219900011>
- Hamada, S.; Ohta, T. 2010. Seasonal variations in the cooling effect of urban green areas on surrounding urban areas, *Urban Forestry & Urban Greening* 9: 15–24. <https://doi.org/10.1016/j.ufug.2009.10.002>
- Herold, M.; Couclelis, H.; Clarke, K. C. 2005. The role of spatial metrics in the analysis and modeling of urban land use change, *Computer, Environment and Urban Systems* 29(4): 369–399. <https://doi.org/10.1016/j.compenvurbsys.2003.12.001>
- Huang, G.; Cadenasso, M. L. 2016. People, landscape, and urban heat island: dynamics among neighborhood social conditions, land cover and surface temperatures, *Landscape Ecology* 31(10): 2507–2515. <https://doi.org/10.1007/s10980-016-0437-z>
- Jantz, C. A.; Goetz, S. J.; Shelley, M. K. 2004. Using the SLEUTH urban growth model to simulate the impacts of future policy scenarios on urban land use in the Baltimore-Washington metropolitan area, *Environment and Planning B: Planning and Design* 31(2): 251–271. <https://doi.org/10.1068/b2983>
- Jimenez-Munoz, J. C.; Sobrino, J. A. 2003. A generalized single channel method for retrieving land surface temperature from remote sensing data, *Journal of Geophysical Research* 108(D22): 2015–2023. <https://doi.org/10.1029/2003JD003480>
- Li, C.; Thinh, N. X. 2013. Investigation and comparison of land-cover change patterns in Xuzhou city, China, and Dortmund city region, Germany, using multitemporal Landsat images, *Journal of Applied Remote Sensing* 7(1): 073458. <https://doi.org/10.1117/1.JRS.7.073458>
- Li, C.; Thinh, N. X.; Zhao, J. 2014. Spatiotemporally varying relationships between urban growth patterns and driving factors in Xuzhou city, China, *Photogrammetrie Fernerkundung Geoinformation* 6: 535–548. <https://doi.org/10.1127/pfg/2014/0246>

- Li, F.; Jackson, T. J.; Kustas, W. P.; Schmugge, T. J.; French, A. N.; Cosh, M. H.; Bindlish, R. 2004. Deriving land surface temperature from Landsat 5 and 7 during SMEX02/SMACEX, *Remote Sensing of Environment* 92: 521–534. <https://doi.org/10.1016/j.rse.2004.02.018>
- Li, J.; Song, C.; Cao, L.; Zhu, F.; Meng, X. 2011. Impacts of landscape structure on surface urban heat islands: a case study of Shanghai, China, *Remote Sensing of Environment* 115: 3249–3263. <https://doi.org/10.1016/j.rse.2011.07.008>
- Li, X.; Zhou, W.; Ouyang, Z. 2013. Relationship between land surface temperature and spatial pattern of greenspace: what are the effects of spatial resolution?, *Landscape and Urban Planning* 114: 1–8. <https://doi.org/10.1016/j.landurbplan.2013.02.005>
- Li, X.; Zhou, W.; Ouyang, Z.; Xu, W.; Zheng, H. 2012. Spatial pattern of greenspace affects land surface temperature: evidence from the heavily urbanized Beijing metropolitan area, China, *Landscape Ecology* 27(6): 887–898. <https://doi.org/10.1007/s10980-012-9731-6>
- Liang, B.; Weng, Q. 2008. Multi-scale analysis of census-based land surface temperature variations and determinants in Indianapolis, United States, *Journal of Urban Planning D-ASCE* 134(30): 129–139. [https://doi.org/10.1061/\(ASCE\)0733-9488\(2008\)134:3\(129\)](https://doi.org/10.1061/(ASCE)0733-9488(2008)134:3(129))
- Lu, D.; Weng, Q. H. 2004. Spectral mixture analysis of the urban landscape in Indianapolis with Landsat ETM+ Imagery, *Photogrammetric Engineering & Remote Sensing* 70(9): 1053–1062. <https://doi.org/10.14358/PERS.70.9.1053>
- Luck, M.; Wu, J. 2002. A gradient analysis of the landscape pattern of urbanization in the Phoenix metropolitan area of USA, *Landscape Ecology* 17(4): 327–339. <https://doi.org/10.1023/A:1020512723753>
- Maimaitiyiming, M.; Ghulam, A.; Tiyip, T.; Pla, F.; Latorre-Carmona, P.; Halik, Ü. 2014. Effects of green space spatial pattern on land surface temperature: implications for sustainable urban planning and climate change adaptation, *ISPRS Journal of Photogrammetry and Remote Sensing* 89: 59–66. <https://doi.org/10.1016/j.isprsjprs.2013.12.010>
- Mallick, J.; Rhaman, A.; Singh, C. K. 2013. Modeling urban heat islands in heterogeneous land surface and its correlation with impervious surface area by using night-time ASTER satellite data in highly urbanizing city, Delhi-India, *Advances in Space Research* 52(4): 639–655. <https://doi.org/10.1016/j.asr.2013.04.025>
- Marceau, D. G. 1999. The scale issue in social and natural sciences, *Canadian Journal of Remote Sensing* 25(4): 347–356. <https://doi.org/10.1080/07038992.1999.10874734>
- Markham, B. L.; Barker, J. L. 1985. Spectral characterization of the LANDSAT thematic mapper sensors, *International Journal of Remote Sensing* 6(5): 697–716. <https://doi.org/10.1080/01431168508948492>
- McGarigal, K.; Cushman, S. A.; Ene, E. 2012. *FRAGSTATS v4: Spatial Pattern Analysis Program for Categorical and Continuous Maps* [online]. Computer software program produced by the authors at the University of Massachusetts, Amherst [cited 8 April 2016]. Available from Internet: <http://www.umass.edu/landeco/research/fragstats/fragstats.html>
- Kikon, N.; Singh, P.; Singh, S. K.; Vyas, A. 2016. Assessment of urban heat islands (UHI) of Noida City, India using multi-temporal satellite data, *Sustainable Cities and Society* 22: 19–28. <https://doi.org/10.1016/j.scs.2016.01.005>
- Kumar, D.; Shekhar, S. 2015. Statistical analysis of land surface temperature-vegetation indexes relationship through thermal remote sensing, *Ecotoxicology and Environmental Safety* 121: 39–44. <https://doi.org/10.1016/j.ecoenv.2015.07.004>
- Oke, T. R. 1982. The energetic basis of the urban heat island, *Quarterly Journal of the Royal Meteorological Society* 108(455): 1–24. <https://doi.org/10.1002/qj.49710845502>
- Patino, J. E.; Duque, J. C. 2013. A review of regional science applications of satellite remote sensing in urban settings, *Computers, Environment and Urban Systems* 37: 1–17. <https://doi.org/10.1016/j.compenvurbsys.2012.06.003>
- Pham, H. M.; Yamaguchi, Y.; Bui, T. Q. 2011. A case study on the relation between city planning and urban growth using remote sensing and spatial metrics, *Landscape and Urban Planning* 100(3): 223–230. <https://doi.org/10.1016/j.landurbplan.2010.12.009>
- Qin, Z.; Karnieli, A.; Berliner, P. 2001. A mono-window algorithm for retrieving land surface temperature from Landsat TM data and its application to the Israel-Egypt border region, *International Journal of Remote Sensing* 22(18): 3719–3746. <https://doi.org/10.1080/01431160010006971>
- Ridd, M. K. 1995. Exploring a V-I-S (Vegetation-Impervious Surface-Soil) model for urban ecosystem analysis through remote sensing: comparative anatomy for cities, *International Journal of Remote Sensing* 16(2): 2165–2185. <https://doi.org/10.1080/01431169508954549>
- Schwarz, N. 2010. Urban form revisited-Selecting indicators for characterising European cities, *Landscape and Urban Planning* 96(1): 29–47. <https://doi.org/10.1016/j.landurbplan.2010.01.007>
- Setiawan, H.; Mathieu, R.; Thompson-Fawcett, M. 2006. Assessing the applicability of the V-I-S model to map urban land use in the developing world: case study of Yogyakarta, Indonesia, *Computers, Environment and Urban System* 30(4): 503–522. <https://doi.org/10.1016/j.compenvurbsys.2005.04.003>
- Sobrino, J. A.; Jiménez-Muñoz, J. C.; El-Kharraz, J.; Gómez, M.; Romaguera, M.; Sòria, M. 2004. Single-channel and two-channel methods for land surface temperature retrieval from DAIS data and its application to the Barrax site, *International Journal of Remote Sensing* 24: 215–230. <https://doi.org/10.1080/0143116031000115210>
- Song, J.; Du, S.; Feng, X.; Guo, L. 2014. The relationships between landscape compositions and land surface temperature: quantifying their resolution sensitivity with spatial regression models, *Landscape and Urban Planning* 123: 145–157. <https://doi.org/10.1016/j.landurbplan.2013.11.014>
- Streutker, D. R. 2002. A remote sensing study of the urban heat island of Houston, Texas, *International Journal of Remote Sensing* 23(13): 2595–2608. <https://doi.org/10.1080/01431160110115023>
- Su, S.; Xiao, R.; Zhang, Y. 2011. Multi-scale analysis of spatially varying relationships between agricultural landscape patterns and urbanization using geographically weighted regression, *Applied Geography* 32(2): 360–375. <https://doi.org/10.1016/j.apgeog.2011.06.005>
- Tu, J. 2011. Spatially varying relationships between land use and water quality across an urbanization gradient explored by geographically weighted regression, *Applied Geography* 31(1): 376–392. <https://doi.org/10.1016/j.apgeog.2010.08.001>
- Voogt, J. A.; Oke, T. R. 1998. Effects of urban surface geometry on remotely-sensed surface temperature, *International Journal of Remote Sensing* 19: 895–920. <https://doi.org/10.1080/014311698215784>
- Voogt, J. A.; Oke, T. R. 2003. Thermal remote sensing of urban climates, *Remote Sensing of Environment* 86: 370–384. [https://doi.org/10.1016/S0034-4257\(03\)00079-8](https://doi.org/10.1016/S0034-4257(03)00079-8)

- Weng, Q. 2009. Thermal infrared remote sensing for urban climate and environmental studies: methods, applications, and trends, *ISPRS Journal of Photogrammetry and Remote Sensing* 64(4): 335–344. <https://doi.org/10.1016/j.isprsjprs.2009.03.007>
- Weng, Y. C. 2007. Spatiotemporal changes of landscape pattern in response to urbanization, *Landscape and Urban Planning* 81(4): 341–353. <https://doi.org/10.1016/j.landurbplan.2007.01.009>
- White, M. A.; Nemani, R. R.; Thornton, P. E.; Running, S. W. 2002. Satellite evidence of phenological differences between urbanized and rural areas of the eastern United States deciduous broadleaf forest, *Ecosystems* 5: 260–277. <https://doi.org/10.1007/s10021-001-0070-8>
- Wu, C. D.; Lung, S. C. C.; Jan, J. F. 2013. Development of a 3-D urbanization index using digital terrain models for surface urban heat island effects, *ISPRS Journal of Photogrammetry & Remote Sensing* 81(7): 1–11. <https://doi.org/10.1016/j.isprsjprs.2013.03.009>
- Wu, J.; Shen, W.; Sun, W.; Tueller, P. T. 2002. Empirical patterns of the effects of changing scale on landscape metrics, *Landscape Ecology* 17: 761–782. <https://doi.org/10.1023/A:1022995922992>
- Yuan, F.; Bauer, M. E. 2007. Comparison of impervious surface area and normalized difference vegetation index as indicators of surface urban heat island effects in Landsat imagery, *Remote Sensing of Environment* 106(3): 375–386. <https://doi.org/10.1016/j.rse.2006.09.003>
- Zhang, H.; Qi, Z.; Ye, X.; Cai, Y.; Ma, W.; Chen, M. 2013. Analysis of land use/land cover change, population shift, and their effects on spatiotemporal patterns of urban heat islands in metropolitan Shanghai, China, *Applied Geography* 44: 121–133. <https://doi.org/10.1016/j.apgeog.2013.07.021>
- Zhou, W.; Huang, G.; Cadenasso, M. L. 2011. Does spatial configuration matter? Understanding the effects of land cover pattern on land surface temperature in urban landscapes, *Landscape and Urban Planning* 102(1): 54–63. <https://doi.org/10.1016/j.landurbplan.2011.03.009>
- Zhou, W.; Qian, Y.; Li, X.; Han, L. 2014. Relationships between land cover and the surface urban heat island: Seasonal variability and effects of spatial and thematic resolution of land cover data on predicting land surface temperatures, *Landscape Ecology* 29(1): 153–167. <https://doi.org/10.1007/s10980-013-9950-5>
- Zhou, W.; Wang, J.; Cadenasso, M. L. 2017. Effects of the spatial configuration of trees on urban heat mitigation: a comparative study, *Remote Sensing of Environment* 195: 1–12. <https://doi.org/10.1016/j.rse.2017.03.043>